LA-UR-12-24091
Approved for public release; distribution is unlimited.

Title:	Test Problem: Tilted Rayleigh-Taylor for 2-D Mixing Studies
Author(s):	Andrews, Malcolm J. Livescu, Daniel Youngs, David L.
Intended for:	Report

Test Problem:
Tilted Rayleigh-Taylor for 2-D Mixing Studies

Authors: Malcolm J. Andrews (XCP-4, LANL), 505-606-1430, mandrews@lanl.gov
David L. Youngs (AWE) , david.youngs@awe.co.uk
Daniel Livescu (CCS-2, LANL), 505-665-1758, livescu@lanl.gov

Date: August 10, 2012

Version: 1.0

Contents

1. Introduction

The "tilted-rig" test problem originates from a series of experiments (Smeeton & Youngs, 1987, Youngs, 1989) performed at AWE in the late 1980's, that followed from the "rocket-rig" experiments (Burrows et al., 1984; Read & Youngs, 1983), and exploratory experiments performed at Imperial College (Andrews, 1986; Andrews and Spalding, 1990). A schematic of the experiment is shown in Figure 1, and comprises a tank filled with light fluid above heavy, and then "tilted" on one side of the apparatus, thus causing an "angled interface" to the acceleration history due to rockets. Details of the configuration given in the next chapter include: fluids, dimensions, and other necessary details to simulate the experiment. Figure 2 shows results from two experiments, Case 110 (which is the source for this test problem) that has an Atwood number of 0.5, and Case 115 (a secondary source described in Appendix B), with Atwood of 0.9 Inspection of the photograph in Figure 2 (the main experimental diagnostic) for Case 110. reveals two main areas for mix development; 1) a large-scale overturning motion that produces a rising plume (spike) on the left, and falling plume (bubble) on the right, that are almost symmetric; and 2) a Rayleigh-Taylor driven mixing central mixing region that has a large-scale rotation associated with the rising and falling plumes, and also experiences lateral strain due to stretching of the interface by the plumes, and shear across the interface due to upper fluid moving downward and to the right, and lower fluid moving upward and to the left. Case 115 is similar but differs by a much larger Atwood of 0.9 that drives a strong asymmetry between a left side heavy spike penetration and a right side light bubble penetration. Case 110 is chosen as the source for the present test problem as the fluids have low surface tension (unlike Case 115) due the addition of a surfactant, the asymmetry small (no need to have fine grids for the spike), and there is extensive reasonable quality photographic data. The photographs in Figure 2 also reveal the appearance of a boundary layer at the left and right walls; this boundary layer has not been included in the test problem as preliminary calculations suggested it had a negligible effect on plume penetration and RT mixing.

The significance of this test problem is that, unlike planar RT experiments such as the Rocket-Rig (Youngs, 1984), Linear Electric Motor - LEM (Dimonte, 1990), or the Water Tunnel (Andrews, 1992), the Tilted-Rig is a unique two-dimensional RT mixing experiment that has experimental data and now (in this TP) Direct Numerical Simulation data from Livescu and Wei. The availability of DNS data for the tilted-rig has made this TP viable as it provides detailed results for comparison purposes. The purpose of the test problem is to provide 3D simulation results, validated by comparison with experiment, which can be used for the development and validation of 2D RANS models. When such models are applied to 2D flows, various physics issues are raised such as double counting, combined buoyancy and shear, and 2-D strain, which have not yet been adequately addressed. The current objective of the test problem is to compare key results, which are needed for RANS model validation, obtained from high-Reynolds number DNS, high-resolution ILES or LES with explicit sub-grid-scale models. The experiment is incompressible and so is directly suitable for algorithms that are designed for incompressible flows (e.g. pressure correction algorithms with multi-grid); however, we have extended the TP so that compressible algorithms, run at low Mach number, may also be used if careful consideration is given to initial pressure fields. Thus, this TP serves as a useful tool for incompressible and compressible simulation codes, and mathematical models.

In the remainder of this TP we provide a detailed specification; the next section provides the underlying assumptions for the TP, fluids, geometry details, boundary conditions (and alternative set-ups), initial conditions, and acceleration history (and ways to treat the acceleration ramp at the start of the experiment). This is followed by a section that defines data to be collected from the simulations, with results from the experiments and DNS from Livescu using the CFDNS code, and ILES simulations from Youngs using the compressible TURMOIL code and Andrews using the incompressible RTI3D code. We close the TP with concluding remarks, and Appendices that includes details of the sister Case 115, initial condition specifications for density and pressure fields.

2. Problem definition

2.1 Geometry and Fluids

Figure 1 is a schematic of the experimental tank showing definitions of dimensions, angle definitions and accelerations. The tank dimensions are given in Table 1; in Case 110 the actual tank vertical dimension was 25 cm with an air bubble trap at the top of tank. A rectangular tank height of 24cm should adequately account for this. Preliminary calculations have shown that the 2.5cm depth has negligible effect on the growth of the central RT mix zone, or the left/right plume development. For the test problem a tank depth of 15 cm (i.e. 6x the experimental one) should be used to give better statistical averages for the RANS model comparison and provide data unaffected by two-dimensional effects.

The fluids used in Case 110 were NaI solution and Hexane. Fluid properties may be found in Table 2.

2.2 Boundary conditions

We choose not to include viscous wall effects in the boundary conditions. The experimental results suggest that wall effects do have some influence. However, we do not wish to include these effects in the RANS models. Hence the 3D calculations use either free-slip or cyclic boundaries to facilitate ensemble averaging for comparisons with RANS models. We specify two sets of boundary conditions as some computer simulation codes may have hard-wired cyclic boundaries (e.g. spectral HPC codes), the two sets of possible boundary conditions, as shown in Figure 3:

1) For codes that can specify free-slip BCs the left/right and top/bottom walls are free-slip, with the front and back as cyclic, see Figure 3 (left).

2) For codes that require cyclic boundary conditions for left/right boundaries we double the width of the domain so the tilted interface becomes a complete "saw-tooth" giving left/right symmetry, the front/back walls are cyclic, and the top/bottom are free-slip; see Figure 3 (right).

2.3 Initial Conditions

There are two main initial conditions, the density interface (to take into account the tilt and initial density perturbations), and the pressure field.

Density interface: the mean position is specified as shown in Figure 3, with the dimensions/angles of Table 1. Interface height perturbations are superimposed as a k^{-2} spectrum ($k=2\pi/\lambda$), with λ_{min}=0.2cm, $\lambda_{max}=L_x/2$=7.5cm, and standard deviation=0.001 λ_{max}. (values need to be confirmed by running simulations). The random perturbation can be calculated by using the subroutine PERTINT from the IWPCTM11 web site (http://laws.lanl.gov/IWPCTM11/TP_2_pertint.txt). In that case the input required is SS=-2.0, XLMIN=0.2, XLMAX=7.5, SD=0.0075. The interface height (tilt + perturbation) defines the fluid volume fractions, f_1, f_2, for each cell and hence the initial density: $\rho = f_1\rho_1 + f_1\rho_2$; alternatively for DNS one could use the same PERTINT routine but initialize the density perturbations through an error function, as described in the Appendix, to ensure the smoothness of the profile. Calculations should also be run with the tilt-angle set to zero i.e. random perturbations only, in order to assess the 2D effect on the amount of mixing.

Initial velocity fields are set to zero. For incompressible simulations the initial pressure field is set up by the Poisson solver during the first time-step. For compressible simulations, a suitable constant gravity, g , should be used rather that the time-vary g recorded for the experiment (g was approximately constant for most of the experimental period). Time-varying g is not recommended here for compressible simulations in order to avoid the global adjustment to the pressure field needed throughout the simulation. In this case we recommend a suitable Poisson equation should be solved for the initial pressure field. The details are given in Appendix 5.1; 2-D and 3-D Poisson solvers are will be provided in Version 2 of the TP (Fall 2012) to facilitate 3-D ILES simulations, and 2-D RANS models. Compressible simulations with variable acceleration are possible if a much lower Mach (~0.02) number is used and this may be a feasible approach for 2-D RANS models.

2.4 Computational Grids and Time Steps for Case 110

2.4.1 Overview

For the tank cross-section, L_x = 15cm and L_y = 15 cm is recommended and serves as the reference case for all the results reported below (variations are also discussed in the next section). The tank height, L_z , may either correspond to the experimental situation or exceed this. Most of the output requested is unaffected by the upper and lower boundaries and increasing L_z should facilitate the use of powers of 2 for the grid sizes. It is recommended that the number of cells in the x-direction should be at least 512. Two different mesh sizes should be used in order to examine mesh convergence.

2.4.2 Andrews simulations with RTI3D

Andrews used the following grids for the ILES calculations:

a) Case 110: $N_x * N_y * N_z = 320 * 320 * 480$, $\Delta x * \Delta y * \Delta z = (L_x/N_x) * (L_y/N_y) * (L_z/N_z)$
b) Case 110: $N_x * N_y * N_z = 512 * 512 * 768$, $\Delta x * \Delta y * \Delta z = (L_x/N_x) * (L_y/N_y) * (L_z/N_z)$

For the reference case the aim was to keep cell sizes similar, while maintaining a power of 2 suitable for a multi-grid pressure algorithm with up to 4 levels of refinement. We note that for the purposes of collecting ensemble averaged data for RANS model validation/development, the "y" dimension could be increased with a corresponding increase in the number of cells An alternative to increasing the y dimension for RANS data is to perform multiple runs using different initial random number seeds for the density perturbations – our experience suggests that this would offer no gain.

Choice of time-step may be automatic according to an accuracy or stability condition. For the grid above Andrews has found that the a time-step of $2*10^{-6}$ secs gives a maximum Courant number during the simulation of about 0.2 .

2.4.3 Livescu simulations with CFDNS

The DNS runs of Livescu used two cross-sections, one corresponding to the experimental set-up (quasi 2-D) and one with the reference square cross-section (3-D):

a) Lx=15 cm, Ly=2.5 cm, with Nx=1536, Ny=256 (the domain reported here)
b) Lx=15 cm, Ly=15 cm, with Nx=1536, Ny=1536 (recommended to provide better statistics)

Since the data provided for model development are obtained by averaging in the y direction, the experimental cross section may not provide enough statistical samples for good averages. Therefore, a square cross-section is more appropriate for obtaining converged averages. In addition, while it is expected that some of the global quantities will be similar for the two cases, there are non-trivial 2-D effects at large scales in the case of the experimental cross-section. This may affect the higher order statistics (e.g. those needed by models like BHR). In order to examine the sensitivity of the results to these two-dimensional effects, we have used the two-cross sections above.

For the two DNS runs, the vertical size of the domain was large, in order to examine long-time effects:

a) Lz= 75 cm
b) Lz= 50 cm

For the DNS runs, the time integration is adaptive and the time step decreases as the flow evolves, from about $7.5*10^{-6}$ s to about $1*10^{-6}$ s. This is of the same order as that used for the ILES calculations by Andrews.

2.4.3 Youngs simulations with TURMOIL

TURMOIL simulations have been run with the following domains and resolutions:

a) Lx= Ly= 15 cm, Lz= 24 cm, 300x300x480 meshes
b) Lx= Ly= 15cm, Lz= 60 cm, 300x300x1200 meshes
c) Lx= Ly= 15cm, Lz= 24 cm, 600x600x960 meshes
d) Lx= Ly= 15cm, Lz= 24 cm, 600x600x960 meshes, no tilt.

Comparison of a) and b) shows the influence of the upper and lower boundaries. For b) the upper and lower boundaries should little effect during the entire simulation. Comparison of a) and c) shows the effect mesh resolution. Calculation d) shows how much mixing occurs if the tilt is not present.

2.6 Acceleration History – Simulation Times

In the experiment the tank acceleration ramped-up during the initial motion and is given in Table 3; note that for Case 110 the acceleration attained a roughly constant value after 12 ms, and for Case 115 after 7ms. The complete acceleration history is available in Table 3 and plotted in Figure 4.

There are two ways to account for the variable acceleration:

1) Incorporate Table 3 directly into the simulation (i.e. a variable "g"), however this may create problems for compressible codes.

2) Constant accelerations may be used instead. Suitable values are g = 0.035cm/ms^2 for Case 110 and g= 0.016cm/ms^2 for Case 115. A non-dimensional time, τ , should be used for comparison with experimental results and with variable –g simulations. This is given by

$$\tau = \int \sqrt{\frac{Ag}{L_x}} dt + \delta$$

where A is the Atwood number and δ is a correction term. For the constant-g simulations δ is zero. For variable-g δ = -0.053 (case 110) and δ=-0.014 (case 115). A simple Layzer-Goncharov model, described in Appendix 5.2 has been used to derive these corrections.

The second method should be used for compressible simulations of the experiment.

With reference to Figure 4, it is recommended that Case 110 be run to 71 ms.

3. Results

3.1 Data To Be Collected

The data to be collected consists of a combination of integral quantities to be plotted as functions of time and two-dimensional plots at selected times. All quantities are unambiguously defined and are suitable for direct comparison with RANS model simulations.

3.1.1 Integral values to be plotted versus non-dimensional time, τ

Let $\bar{\phi}(x,z)$ denote the average of ϕ in the y-direction and let $\bar{\bar{\phi}}(z)$ denote the average of ϕ over an x-y plane. The following integral quantities should be supplied as functions of time for the calculations *with* and *without* the tilt-angle included (except for the mix tilt angle).

1) Left (spike) and right (bubble) plume penetration (H_s and H_b) , see Figure 5. For the calculations with the tilt included, these should be measured to the points where $\bar{\bar{f}}_1 = 0.001$ and $\bar{\bar{f}}_2 = 0.001$. For the calculations without the tilt included, these should be measured to the points where $\bar{\bar{f}}_1 = 0.01$ and $\bar{\bar{f}}_2 = 0.01$.

2) Mix tilt angle, β , see Figure 5. This is derived from the mean interface height calculated as a function of x :

$$h(x) = \int_{z_{min}}^{z_{max}} \bar{f}_1(x,z)dz$$

The tilt angle (in degrees) is then found from a least-squares linear fit to the values of $h(x)$ for central 40% of the *x*-range. This formula should give a good estimate up to stage 2 (section 3.1.2). The side bubble and spike will effect the results at later stages.

3) Integral mix width. For calculations with and without the tilt, this is defined as

$$W = \int \bar{f}_1 \bar{f}_2 dxdz / L_x$$

(for the calculation without the tilt this should be close to $\bar{W} = \int \bar{\bar{f}}_1 \bar{\bar{f}}_2 dz$)

4) Total turbulence kinetic energy, k_{TOT} . This is defined as follows.
The total kinetic energy is

$$K = \tfrac{1}{2}\int \rho \boldsymbol{u}^2 dxdydz = \tilde{K} + k_{TOT}$$

where $k_{TOT} = L_x \int \bar{\rho} k dxdz$

with $$k = \frac{\overline{\rho\left\{(u_x - \tilde{u}_x)^2 + u_y^2 + (u_z - \tilde{u}_z)^2\right\}}}{\bar{\rho}}, \quad \tilde{u}_x = \frac{\overline{\rho u_x}}{\bar{\rho}}, \quad \tilde{u}_z = \frac{\overline{\rho u_z}}{\bar{\rho}}$$

5) Global molecular mixing parameter. This is defined as

$$\Theta = \frac{\int \overline{f_1 f_2} dxdz}{\int \bar{f}_1 \bar{f}_2 dxdz}$$

6) Energy dissipation fraction. This is defined as

$\Delta = \dfrac{D}{D + k_{TOT}}$ where D is the total KE dissipation. D may be calculated from the viscous or sub-grid LES dissipation (or if the change in internal energy is negligible and energy conservation is good, from the relation $P = D + K$ where P is the loss of potential energy).

3.1.2 Two-dimensional plots at selected times

Three times, corresponding to the experimental photographs, are selected for case RT110: t_{exp}=45.3, 59.8 and 71.1 ms (t_{exp}=59.8 is the last experimental time for which the results are unaffected by the upper and lower bound boundaries). The experimental photographs are shown in figure 7. Time t_{exp}=45.3 corresponds to the time when the amount of mixing is about half that at the second time . This final time , t_{exp}=71.1 ms , corresponds to a late-stage photograph. It is anticipated that not all of the 3D simulations will have the appropriate boundary conditions for this. Nevertheless, comparison with 2D RANS models at this time will be useful. The table below gives the values of τ and the equivalent constant-g times (t_{cg}).

stage	τ	t_{exp}	t_{cg}
1	1.256	45.3	37.43
2	1.741	59.8	51.90
3	2.117	71.1	63.11

For calculations with the tilt-angle included, the following 2D plots of y-averaged quantities should be provided.

1) fluid 1 volume fraction, $\overline{f_1}$, (contour values, 0.025,0.3,0.7,0.975).

2) turbulence kinetic energy, k, as defined in section 3.1.1.

3) dissipation rate per unit mass, ε, defined by

$$\varepsilon(x,z) = \frac{\int (\text{dissipation rate per unit volume}) dy}{\int \rho dy}$$

This should be readily available for DNS and LES with explicit sub-grid models (can be obtained from some ILES such as TURMOIL).

4) molecular mixing parameter

$$\theta(x,z) = \frac{\overline{f_1 f_2}}{\overline{f_1}\,\overline{f_2}}$$

5) the b-parameter

$b(x,z) = \overline{\rho' v'}$ where v=1/ρ and the primes denote fluctuations $\phi = \phi - \bar{\phi}$.

6) mass fluxes in horizontal and vertical directions:

$$a_x = \frac{\overline{\rho' u'_x}}{\bar{\rho}}, \qquad a_z = \frac{\overline{\rho' u'_z}}{\bar{\rho}}$$

3.2 TURMOIL results from DLY

Results for the TURMOIL simulations listed in section 2.4.3 are shown in figures 8,9,10 and 11. Figure 11 shows a plot of $\bar{W} = \int \bar{\bar{f}}_1 \bar{\bar{f}}_2 dz$ versus τ for the simulation without tilt . The data points (excluding the early time values) are fitted by the curve:

$h_b = 3.3\bar{W} = \alpha L(\tau + \tau_0)^2$ where τ_0 represents a time-offset.

This gives α=0.048 and quantifies the influence of initial conditions on the problem without tilt. When the tilt is included the amount of mixing, as measured by $W = \int \bar{f}_1 \bar{f}_2 dxdz / L_x$, is increased slightly. Mesh resolution has some effect. The coarser mesh gives slightly more mixing. This is attributed to the reduced dissipation of density and velocity fluctuations at early time when the turbulence is poorly resolved.

Figure 10 shows that the calculated values of H_b and H_s are insensitive to the mesh resolution and are little affected by the upper and lower boundaries until the side bubble/spike gets very close to the boundaries. This is confirmed by the contour plots shown in figure 8(a) and 8(b). Figures 8(a) and 8(c) show similar volume fraction distributions at the two mesh resolutions. However, at the higher mesh resolution, the central mixing zone is somewhat thinner (as expected from figure 11). The experimental values of H_b and H_s are a bit less than the calculated values. Moreover the bubble and spike at the sides of the tank in the experiment tend to pull away from the walls. This difference in behavior is attributed to the influence of the wall boundary layers.

Figure 9 shows contour plots for θ, the molecular mixing parameter, and k, the turbulence kinetic energy at τ=1.741. Note that in the central region θ is higher on the spike side than the bubble side.

3.3 RTI3D results from MJA

Figures 12 through 16 show results from the RTI3D calculations. Units are meters, seconds, kg. Comparison with the results of Youngs reveals good agreement with τ=1.741 corresponding to 60 ms. Comparison of the 320x320x480 and 512x512x768 mesh results reveals a slightly narrower mix region from the 512 mesh.

3.4 CFDNS results from DL

DNS results are shown in figures 8.17 to 8.26 from a variable acceleration quasi-2D run, with Lx, Ly, and Lz: 0.15, 0.025 (Lx and Ly match the experimental values), and 0.75 [m], respectively, on a mesh size of 1536 x 256 x 9600. At the time of the writing both the full 3D (with square cross-section) and quasi-2D cases are still running.

3.5 Comparison of results

Figure 27 shows a comparison of the global molecular parameter obtained from the three codes. The trends are similar in each case. The initial values are high, close to unity for the DNS which solves the initial interface. The parameter then drops and finally rises to a plateau when the "mixing transition" is passed. The final values are higher in the quasi-2D DNS than in the ILES. It is believed that this difference will be resolved when results for the square cross-section DNS are available.

4. Conclusions

The Tilted-Rig Test Problem is intended to serve as a validation problem for RANS models, and as such we have provided ILES and DNS simulations in support of the test problem definition. The generally good agreement between experiment, ILES and DNS supports our assertion that the Tilted-Rig is useful, and the only 2-D TP that can be used to validate RANS models.

This Version 1.0 is expected to be superseded by Version 2.0 in the Fall of 2012; Version 2.0 will present DNS data taken over the 15cmx15cm cross section, and have various Poisson solvers in the Appendices.

5. Appendices

5.1 Initial conditions for compressible codes

For compressible simulations the initial pressure field should be found (as for incompressible simulations) by solving the Poisson equation:

$$\nabla\left(\frac{1}{\rho}\nabla p\right)=0 \quad \text{with } \frac{\partial p}{\partial x}=\rho g \text{ at the upper and lower boundaries}$$

The influence of compressibility is reduced if adiabatic variation is assumed within each fluid (i.e. neutral stability within each fluid). This can be incorporated into the Poisson equation as proposed by Joanne Holford (Holford et al. 2003). Let $\rho_0 = f_1\rho_1 + f_1\rho_2$ denote the density which would be used in an incompressible simulation. Then for the adiabatic variation the pressure is given by

$$\frac{p}{p_0}=\left(\frac{\rho}{\rho_0}\right)^{\gamma} \quad \text{with } p_0 = \text{ initial interface pressure and } \gamma=\tfrac{5}{3}$$

The Poisson equation can then be written in the form

$$\nabla\left(\frac{1}{\rho_0}\nabla p^*\right)=0 \quad \text{with } p^*=\frac{\gamma}{\gamma\text{-}1}p_0^{\frac{1}{\gamma}}p^{\frac{\gamma-1}{\gamma}} \quad \text{and } \frac{\partial p^*}{\partial x}=\rho_0 g \quad \text{at the upper and lower boundaries}$$

A standard Poisson solver may then be used to find the initial pressure field.

If gm-cm-ms units are chosen then the unit for pressure is the bar. The recommended interface pressure for compressible simulations is $p_0 = 20$ bar. This should give a peak Mach number of ~0.25 and increasing the pressure should have little effect.

5.2 A simple model for the influence of variable acceleration

The influence of the variable acceleration on single mode RT growth (wavelength λ) may be found by combining Layzer's equation for bubble growth at A=1 with Gonchorov's limiting bubble a spike velocities for arbitrary A:

bubble(spike) velocity $V=\dfrac{dh}{dt}$

$$(2+E)\frac{dV}{dt}=(1-E)Ag\text{-}\frac{C_dV^2}{\lambda} \qquad \text{where } E=\exp\left(\text{-}\frac{6\pi h}{\lambda}\right)$$

$$\text{and} \quad C_d=\begin{cases}3\pi(1+A) & \text{bubble}\\ 3\pi(1-A) & \text{spike}\end{cases}$$

The model is approximate but the derivation does not assume that g is constant. The above equations are solved for constant g and for the experimental time variation, using values of λ typical of the large scale overturning motion. Results are shown here for case 110 with $\lambda = L_x$ and $h_0 = \frac{1}{2}L_x \tan\theta$. Bubble and spike distances are plotted against the non-dimensional time , τ, defined in section 2.6. If the correction δ = -0.053 is used the variable-g results overlay the constant-g results.

6. References:

Smeeton, V. S., and Youngs, D.L., "Experimental Investigation of Turbulent Mixing by Rayleigh-Taylor Instability, III", AWE Report No. O 35/87, 1987.

Youngs, D. L., " Modelling Turbulent Mixing by Rayleigh-Taylor Instability", *Physica D*, vol. 3, pp270-287, 1989.

Burrows, K. D., Smeeton, V. S., and Youngs, D.L., "Experimental Investigation of Turbulent Mixing by Rayleigh-Taylor Instability, II", AWE Report No. O 22/84, 1984.

Read, K. I., and Youngs, D.L., “Experimental Investigation of Turbulent Mixing by Rayleigh-Taylor Instability”, AWE Report No. O 11/83, 1984.

Andrews, M.J. and Spalding, D.B., "A Simple Experiment to Investigate Two-Dimensional Mixing by Rayleigh-Taylor Instability," *Physics of Fluids A*, Vol. 2, No. 6, pp. 922-927, 1990.

Andrews, M.J., "Turbulent Mixing by Rayleigh-Taylor Instability," Ph.D. Thesis, *London University*, 1986.

Holford, J.M., Dalziel, S. B., and Youngs, D.L., “Rayleigh-Taylor instability at a tilted interface in laboratory experiments and numerical simulations”, *Laser and Particle Beams*, vol.21, pp419-423 , 2003.

7. Tables

Case	L_x	L_y	L_z	Θ (deg)	L_c
110	15.0 cm	2.5 cm	24.0 cm	5^o 46' (5.76667^o)	12.0 cm
115	15.0 cm	5.0 cm	20.0 cm	5^o 9' (5.15^o)	8.3 cm

Table 1. Geometry definitions

Case	Fluid	Density	Viscosity	Surface Tension	Atwood $\frac{\rho_1 - \rho_2}{\rho_1 + \rho_2}$
110	Fluid 1: NaI solution	1.89 g/cm^3	3.3 mN s/m^2	-	0.482
	Fluid 2: Hexane	0.66 g/cm^3	0.31 mN s/m^2		
115	Fluid 1: Pentane	0.626 g/cm^3	0.23 mN s/m^2	13.7 mN/m	0.903
	Fluid 2: Compressed SF_6	0.0319 g/cm^3			

Table 2. Fluid properties

Case 110	Case 115
# RT110 acceleration versus time # adjusted to match measured tank distance versus time # assumes linear interpolation between data points # g=gravity to be used RT simulations # tank acceleration = g+g0 (acceleration used to calculate tank distance) # g0=0.00980665 mm/ms**2 : gravitational acceleration # t(ms) acceleration(g/g0) 0.0 0.000 2.0 0.000 3.0 1.018 4.0 3.258 5.0 6.515 6.0 10.180 7.0 14.150 8.0 18.019 9.0 21.582 10.0 24.636 11.0 26.875 12.0 28.809 13.0 30.540 14.0 32.067 15.0 33.187 16.0 34.103 17.0 34.816 18.0 35.426 19.0 35.732 20.0 36.037 21.0 36.343 22.0 36.444 23.0 36.546 24.0 36.750 25.0 36.648 80.0 34.510 81.0 34.307 82.0 34.103 83.0 33.289 84.0 32.169 85.0 30.744	# RT115 acceleration versus time # adjusted to match measured tank distance versus time # assumes linear interpolation between data points # g=gravity to be used RT simulations # tank acceleration g1=g+g0(acceration used to calculate tank distance) # g0=0.00980665 mm/ms**2 : gravitational acceleration # t(ms) acceleration(g/g0) 0.0 0.000 2.6 0.000 3.6 0.211 4.6 5.174 5.6 11.405 6.6 15.101 7.6 17.213 8.6 18.163 9.6 18.374 10.6 18.058 11.6 17.530 12.6 17.318 13.6 17.213 14.6 17.107 77.6 16.579 78.6 16.474 79.6 16.051 80.6 15.523 81.6 14.784 82.6 13.728 83.6 12.672 84.6 11.405

Table 3. Acceleration history

8. Figures

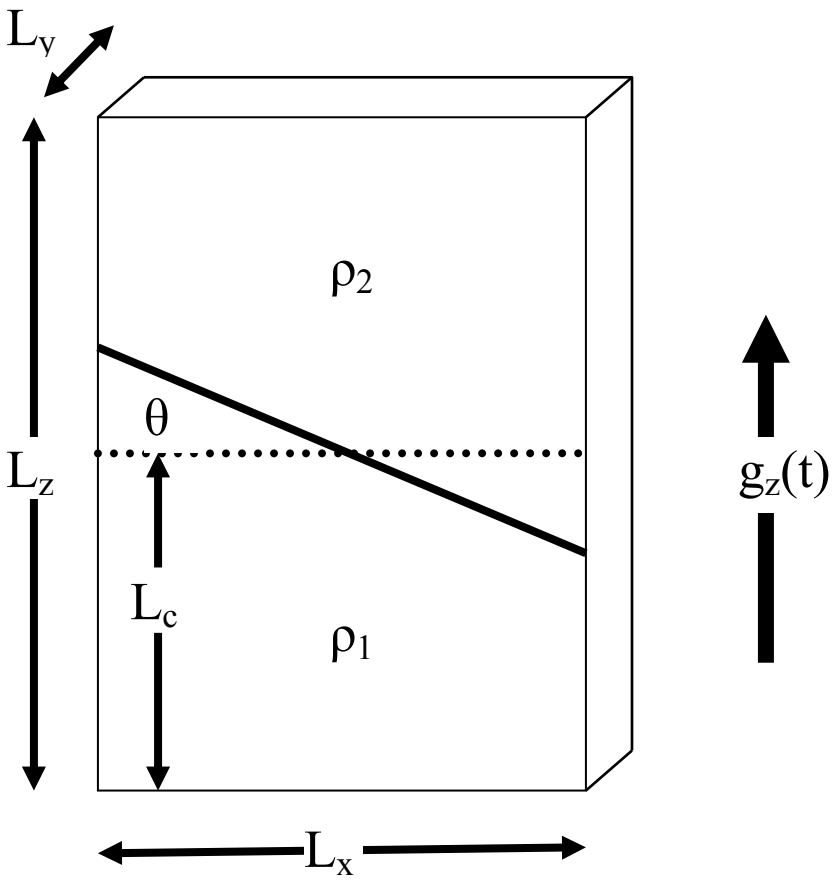

Figure 1. Schematic of the Tilted-Rig Experiment

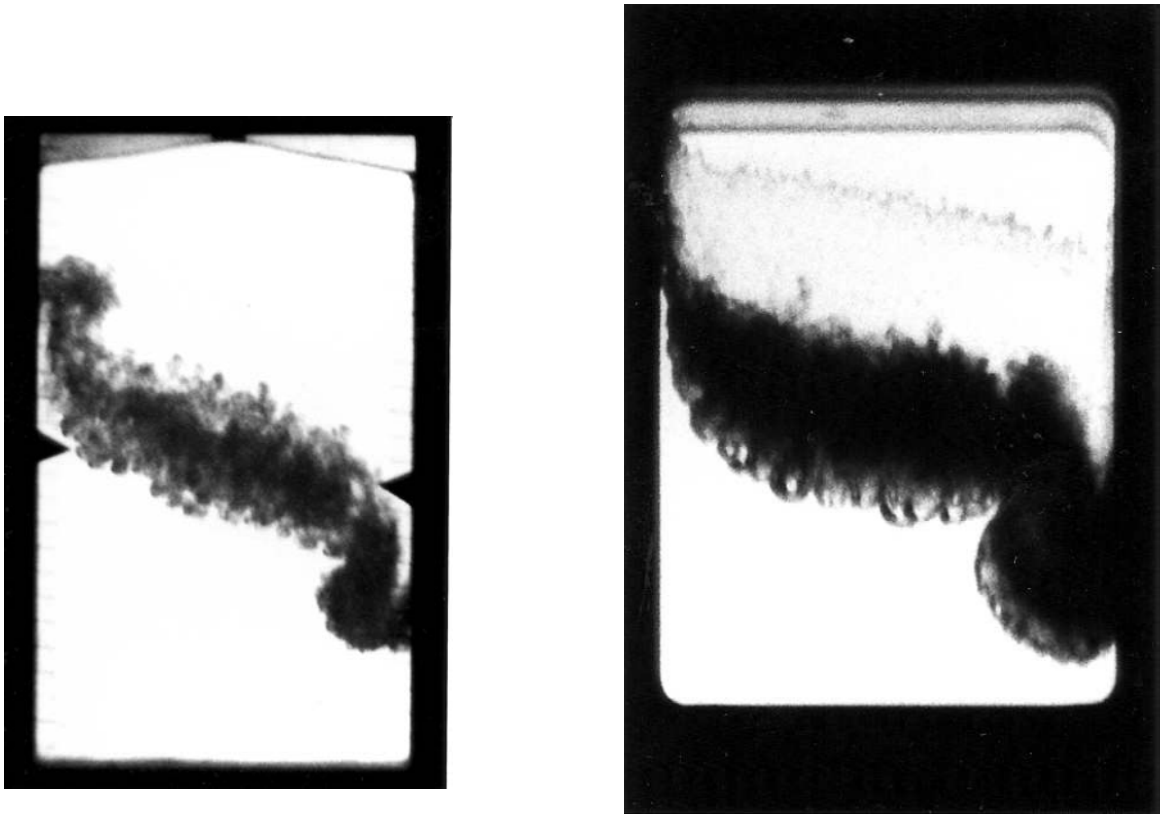

Figure 2. Case 110 (right) and Case 115 (left)

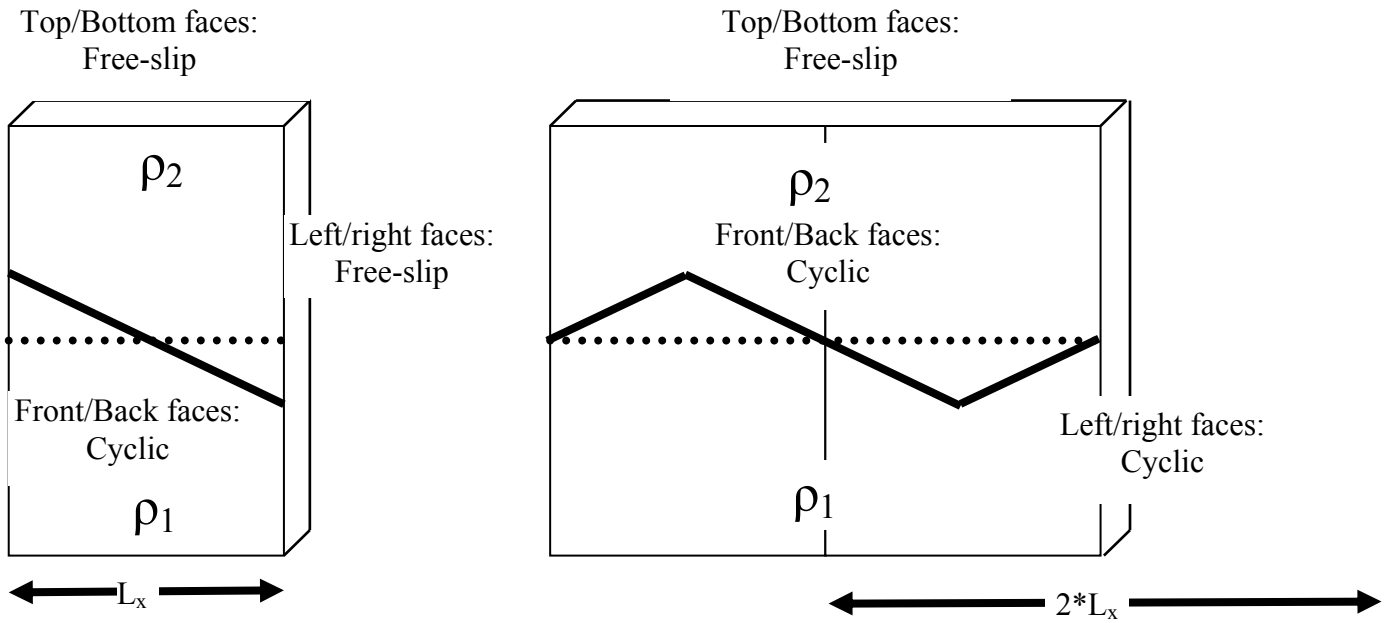

Figure 3. Boundary Conditions; left is for left/right free-slip; right is for equivalent left/right cyclic – note saw-tooth of density interface.

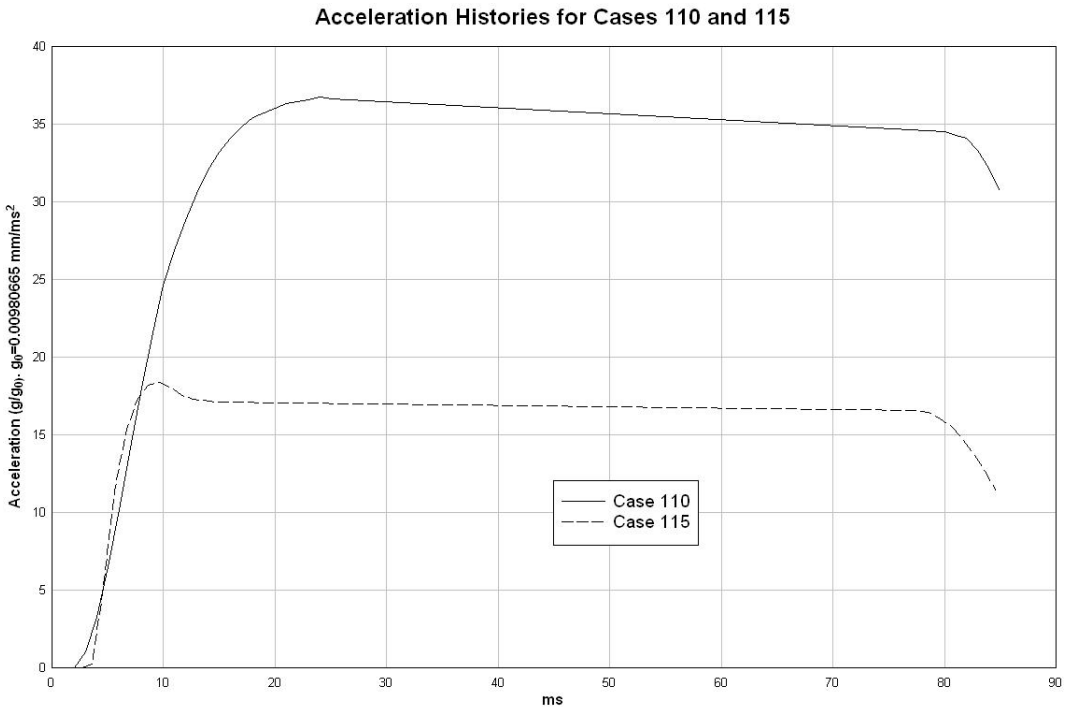

Figure 4. Acceleration histories for Case 110 and 115

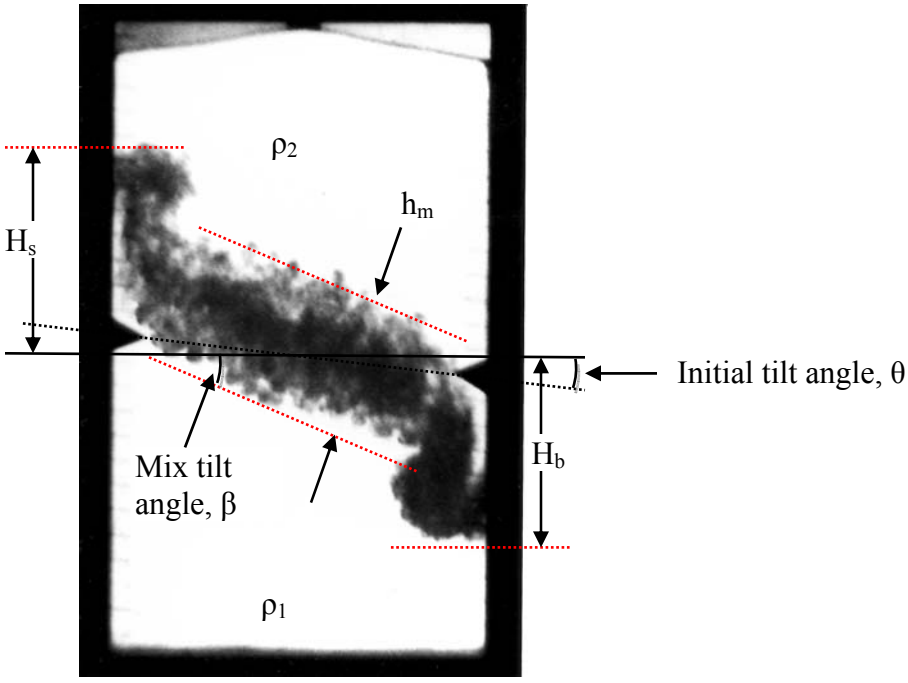

Figure 5. Definition of measurement quantities: H_s, H_b, h_m, β

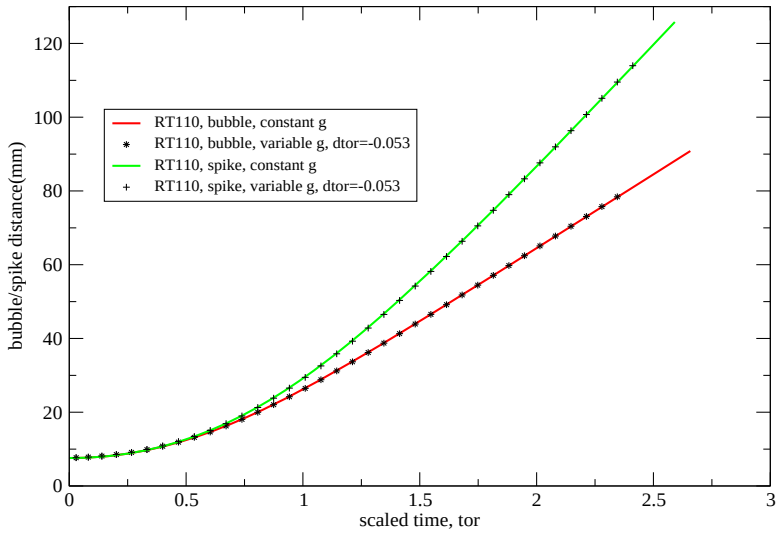

Figure 6. Layzer equation model: Bubble and spike distances for case110.

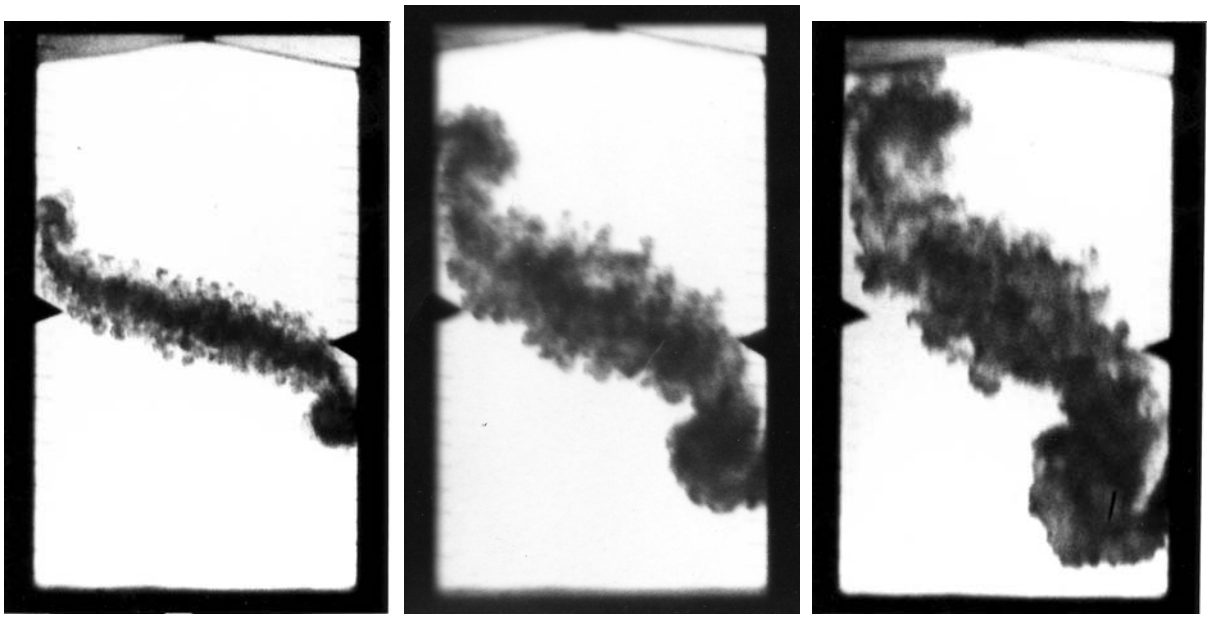

t_{exp} =45.3 ms, τ=1.256 t_{exp} =59.8 ms, τ=1.741 t_{exp} =71.1 ms, τ=2.117

Figure 7: Case 110. Stages selected for comparison with numerical simulations.

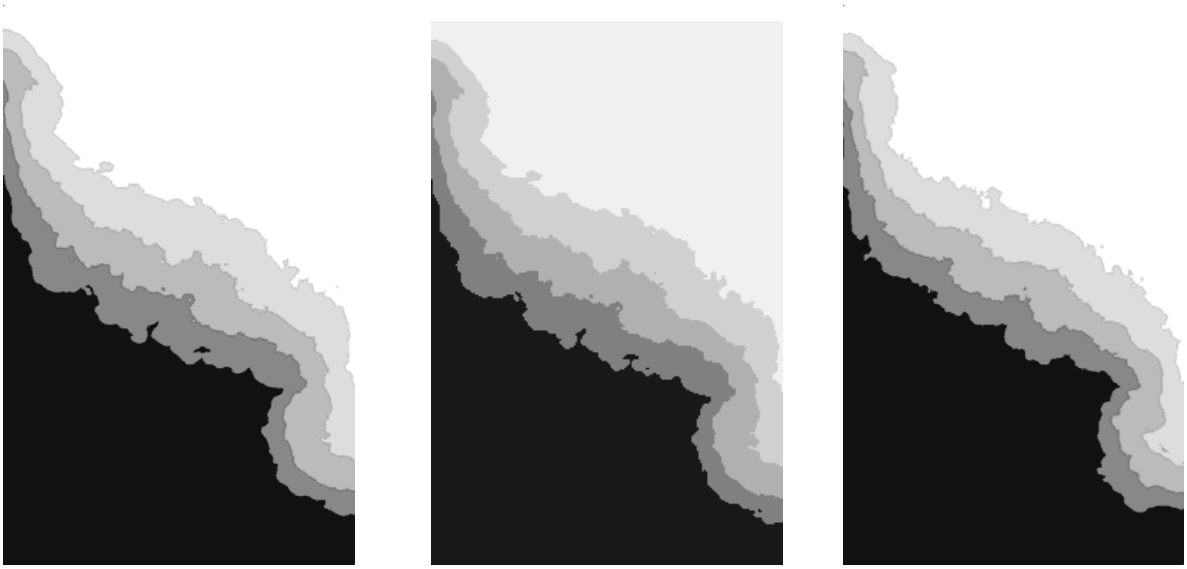

(a) (b) (c)

Figure 8: TURMOIL volume fraction distributions at τ=1.741 (a) 300x300x480 meshes. (b) 300x300x1200 meshes (clipped image). (c) 600x600x960 meshes. Contour levels 0.025, 0.3, 0.7, 0.975.

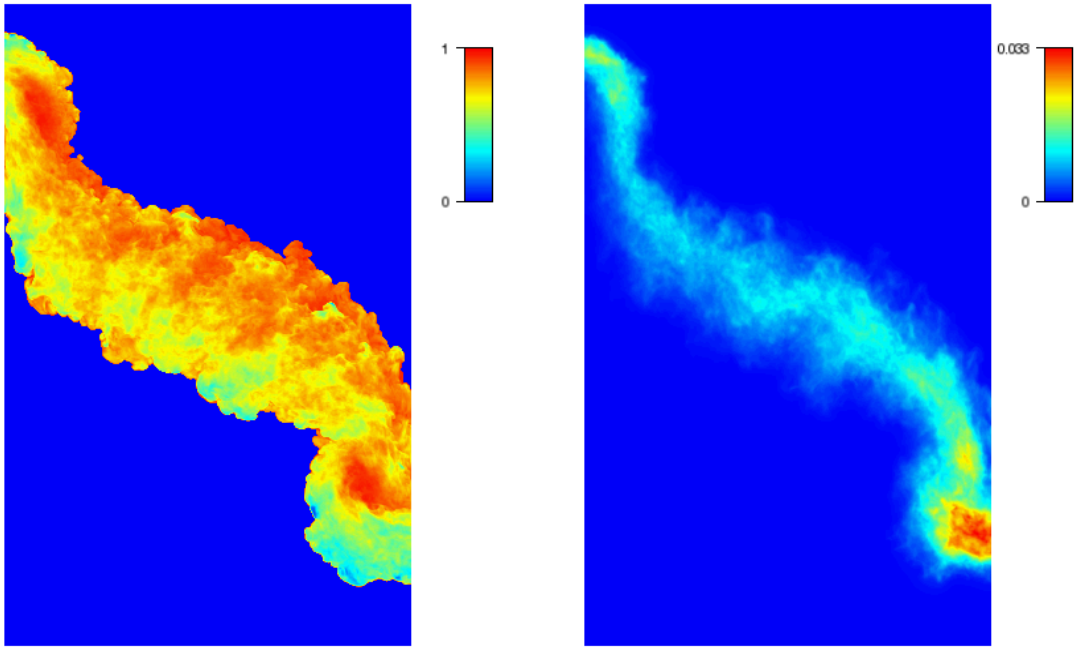

(a) (b)

Figure 9: TURMOIL results for 600x600x960 meshes at τ = 1.741. (a) molecular mixing parameter, θ, (b) turbulence kinetic energy, k, scale maximum =0.033 cm^2/ms^2.

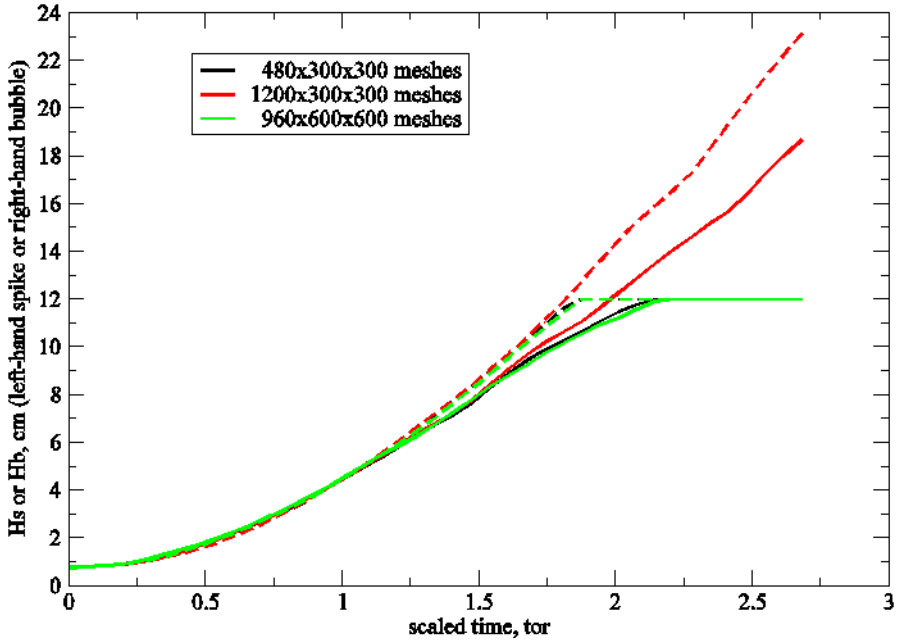

Figure 10: TURMOIL side-wall bubble and spike positions, H_b , Hs versus τ.

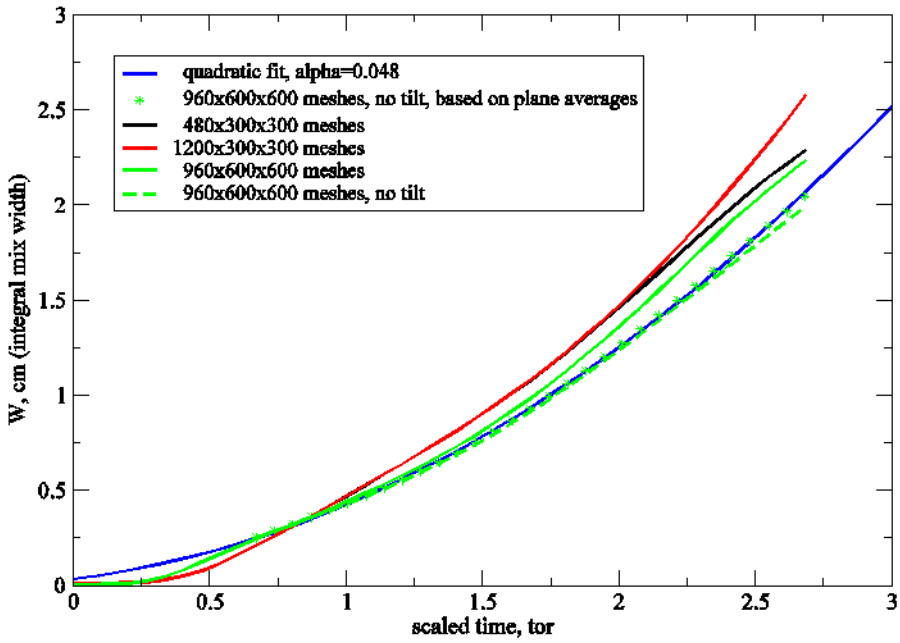

Figure 11: TURMOIL integral mix widths

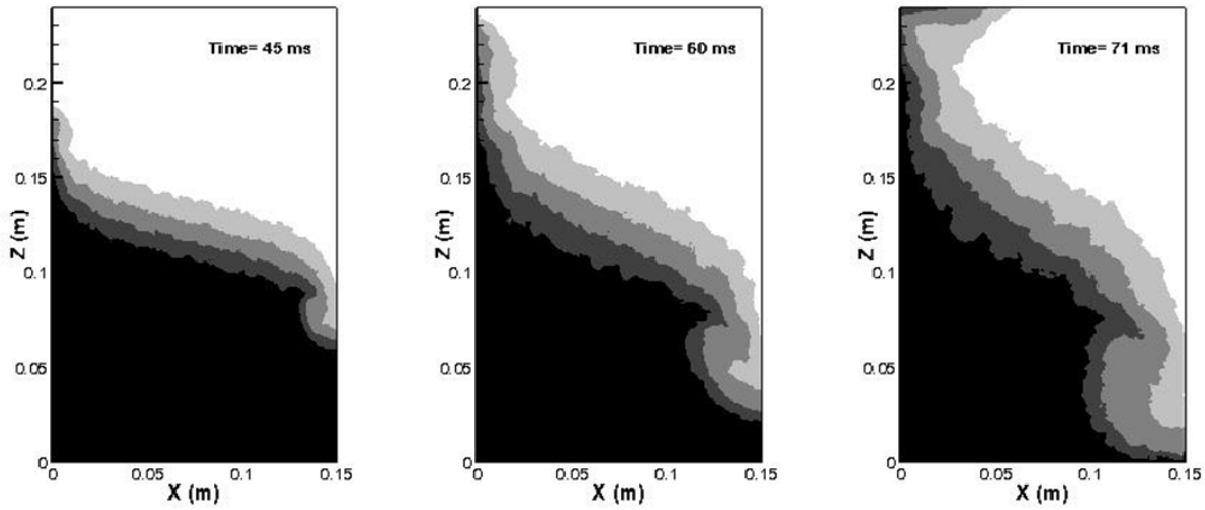

Figure 12a: RTI3D volume fraction distributions at 45 ms, 60 ms and 71 ms using a 512x512x768 mesh with contour levels of 0.025, 0.3, 0.7, 0.975.

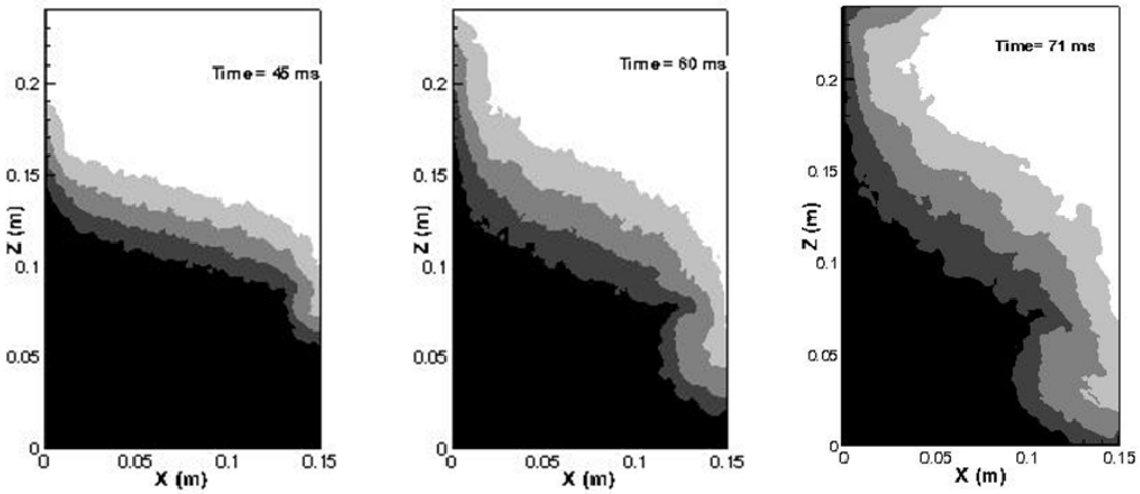

Figure 12b: RTI3D volume fraction distributions at 45ms, 60ms and 71ms using a 320x320x480 mesh with contour levels of 0.025, 0.3, 0.7, 0.975.

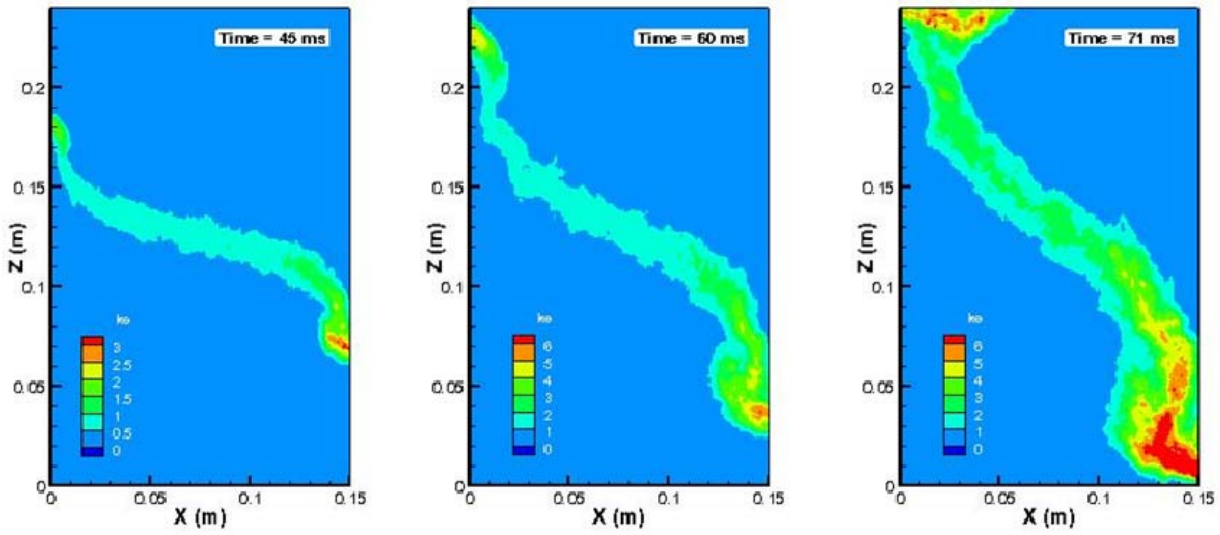

Figure 13a: RTI3D "ke" distributions at t=45, 60 and 71 ms using a 512x512x768 mesh

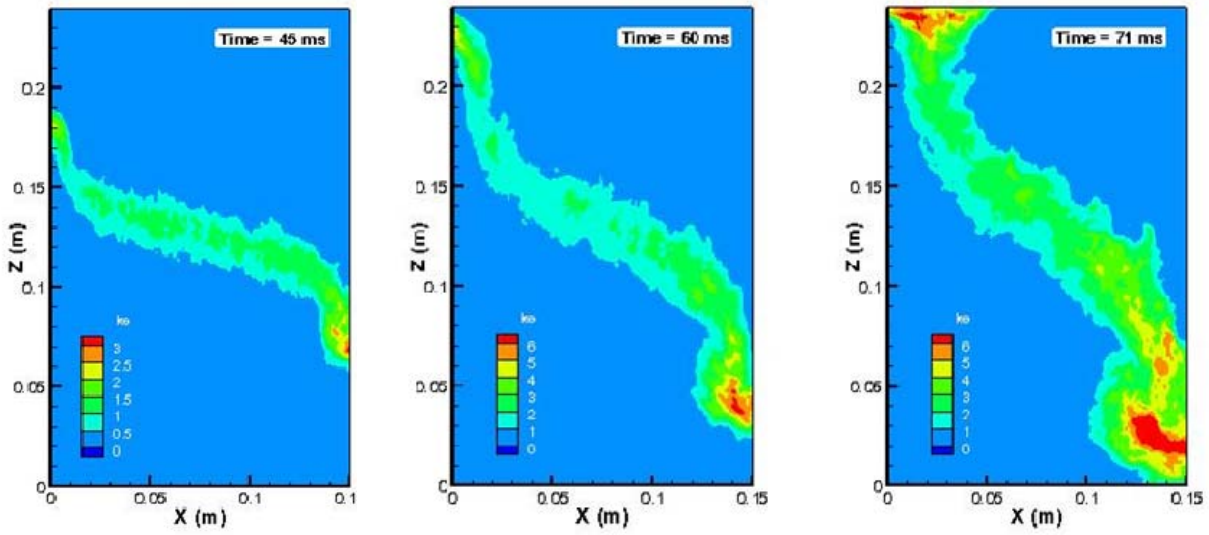

Figure 13b: RTI3D "ke" distributions t= 45ms, 60 ms and 71 ms using a 320x320x480 mesh

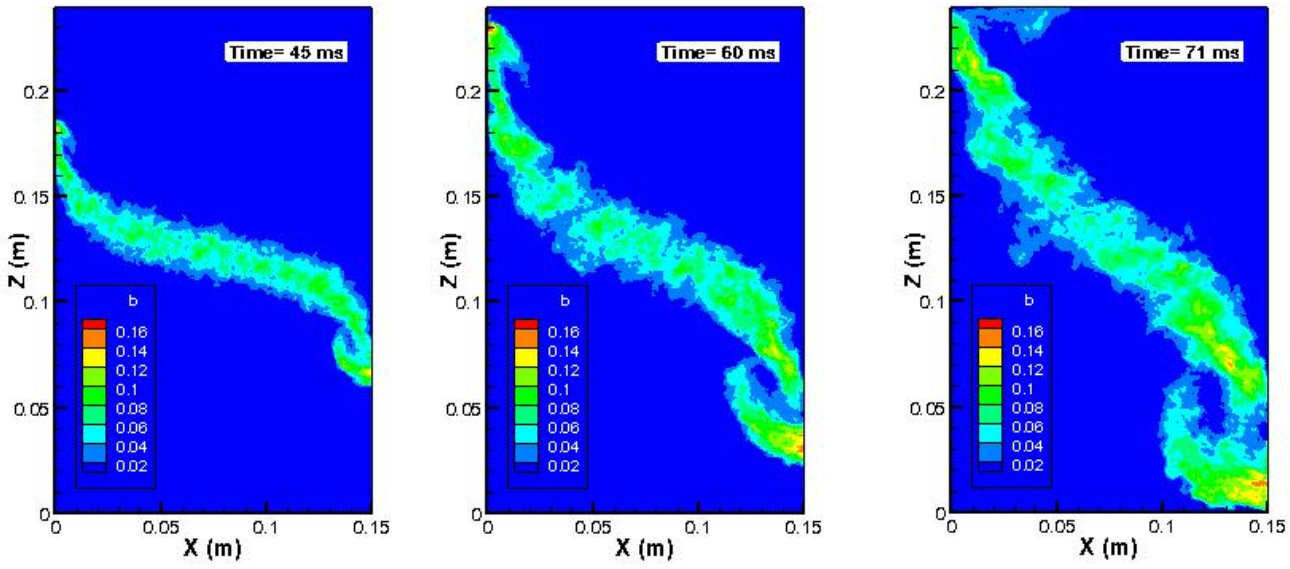

Figure 13c: RTI3D "b" distributions at t=45ms, 60 ms and 71 ms using a 512x512x768 mesh

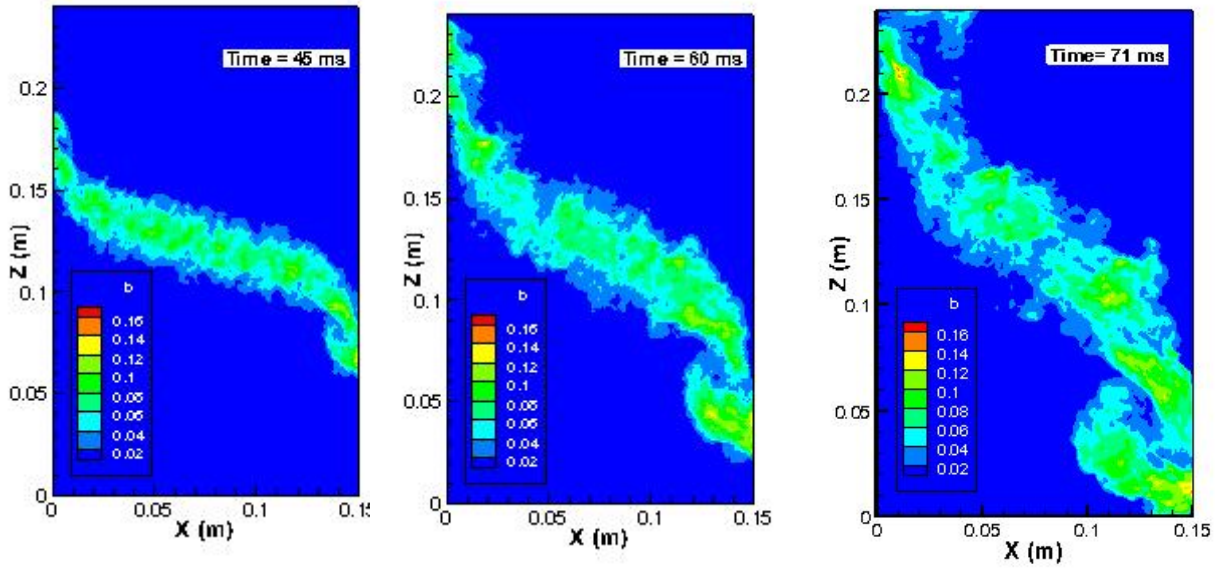

Figure 13d: RTI3D "b" distributions at t= 45ms, 60 ms and 71 ms using a 320x320x480 mesh

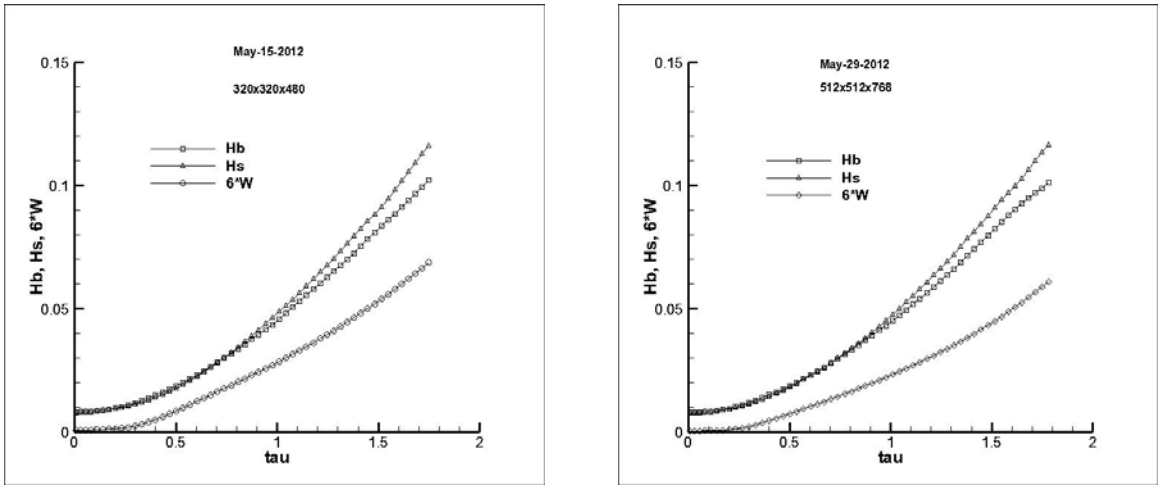

Figure 14: RTI3D side-wall bubble and spike positions, H_b , Hs and 6W (meters) vs. tau for 320x320x480 and 512x512x768 meshes

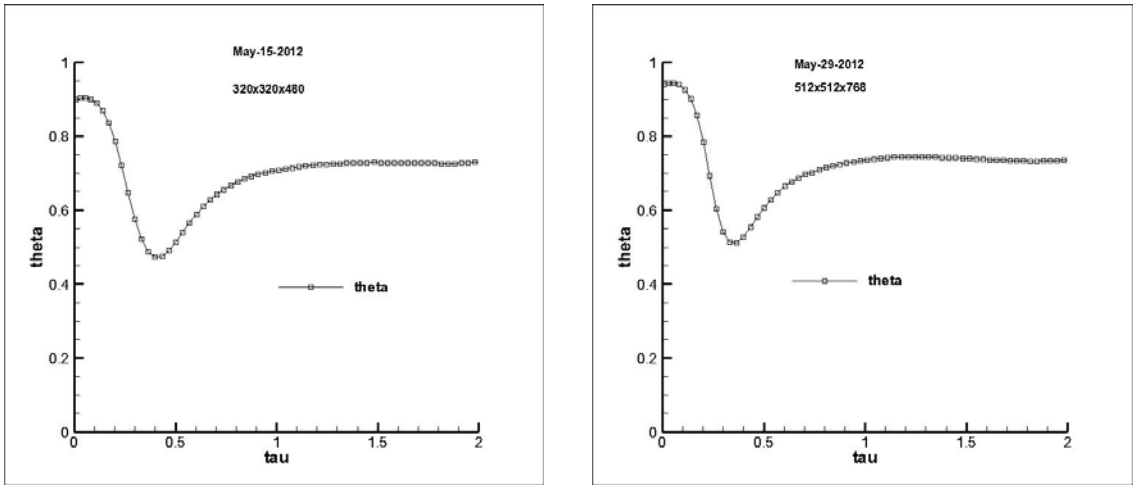

Figure 15: RTI3D theta vs. tau for 320x320x480 and 512x512x768 meshes

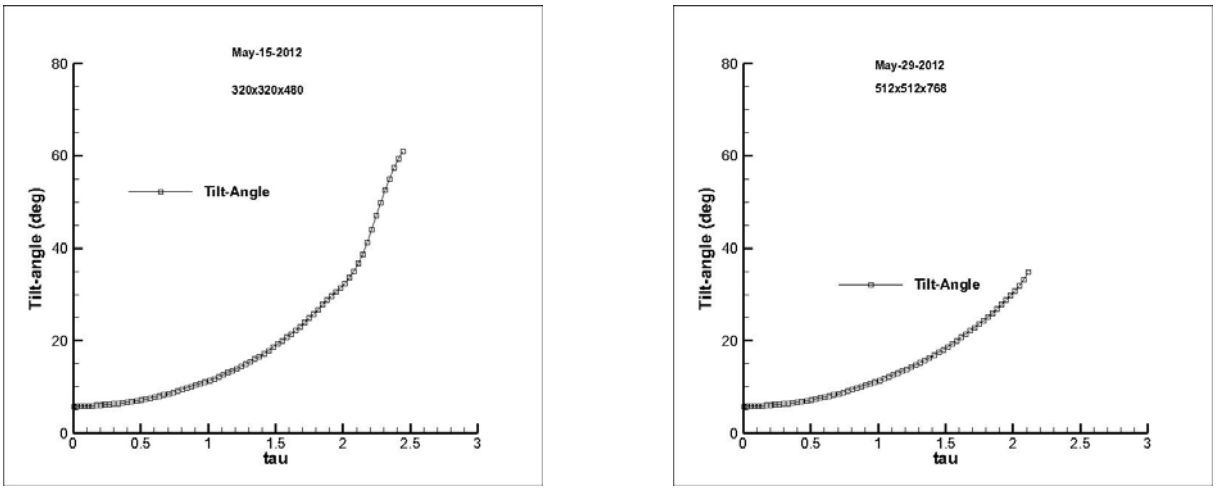

Figure 16: RTI3D tilt-angle vs. tau for 320x320x480 and 512x512x768 meshes

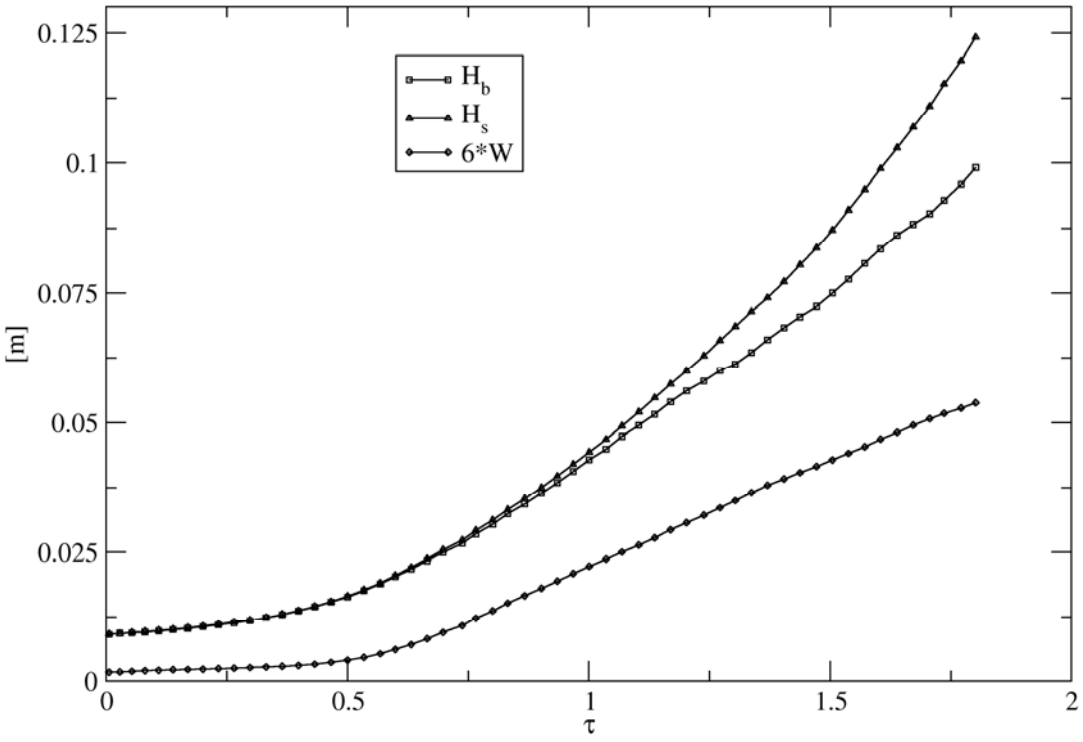

Figure 17: CFDNS side wall bubble and spike height and 6*W for the quasi-2D run.

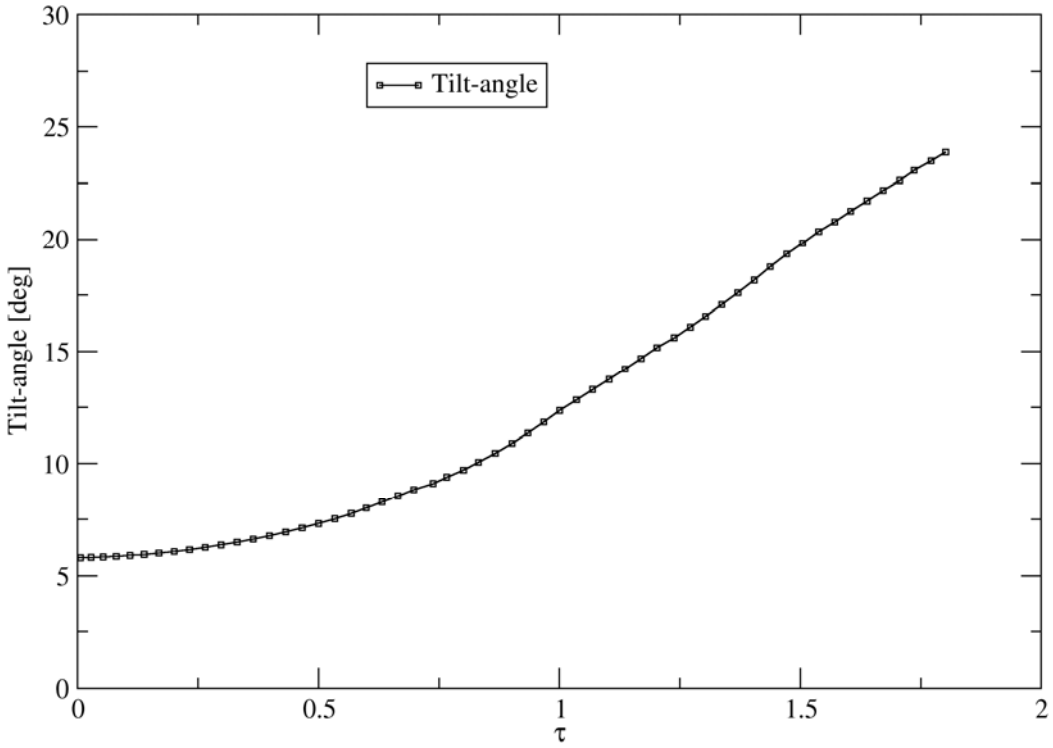

Figure 18: Tilt-angle [degrees] for the quasi-2D run.

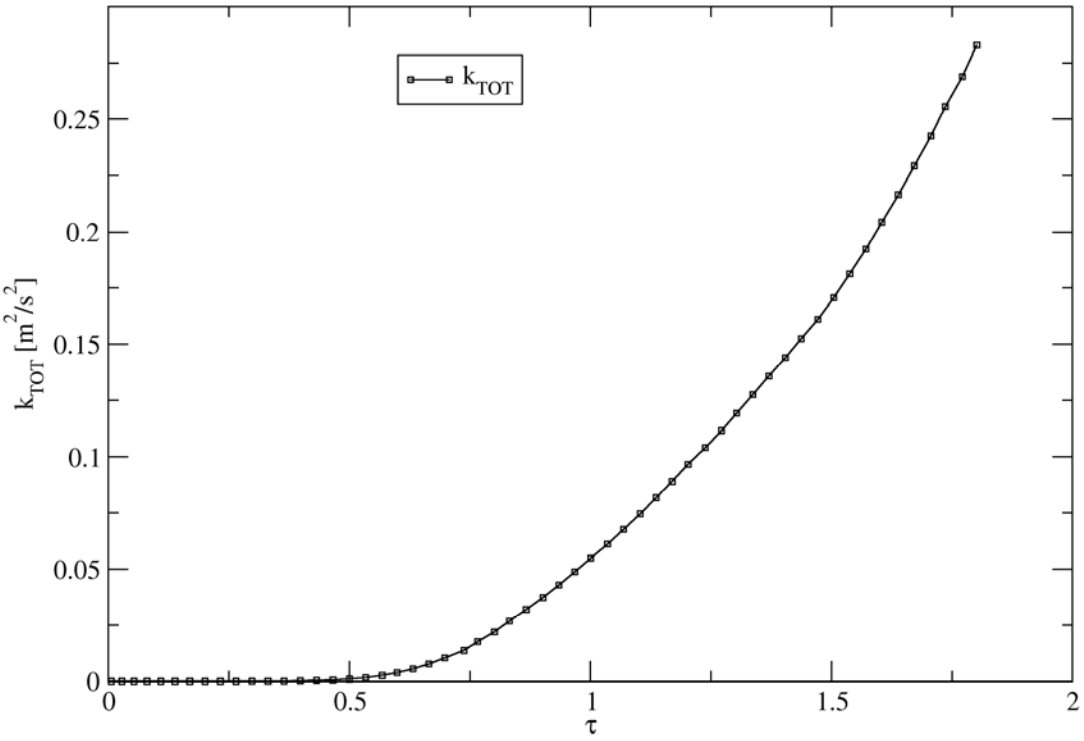

Figure 19: CFDNS kinetic energy and turbulent kinetic energy for the quasi-2D run.

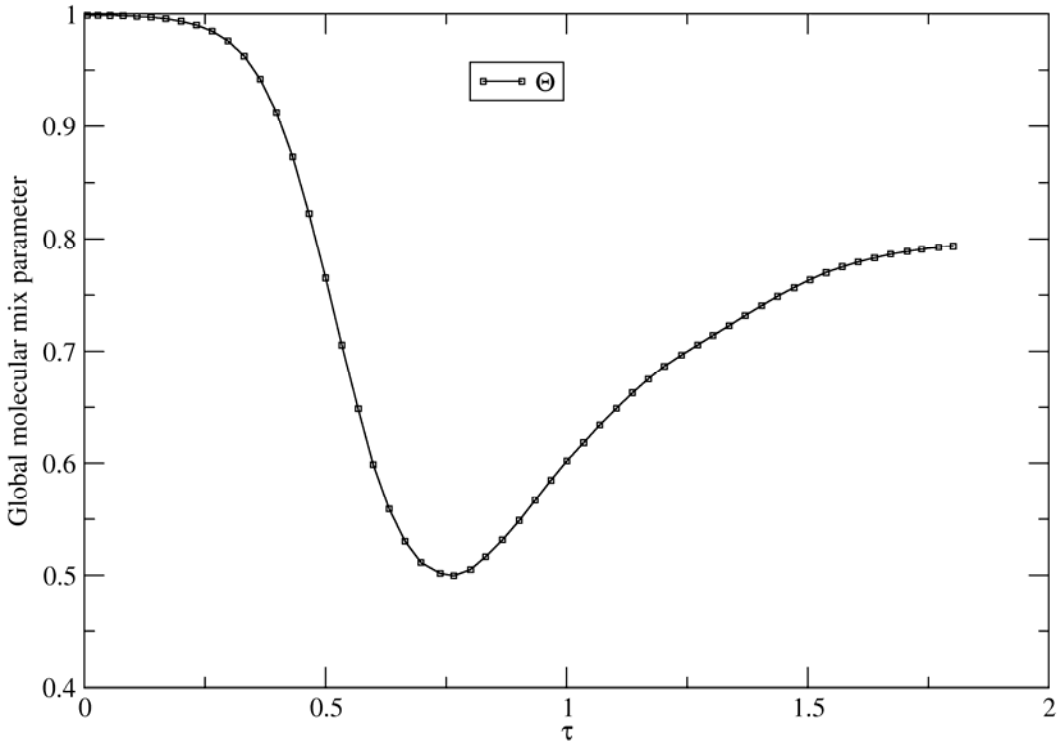

Figure 20: CFDNS global mix parameter for the quasi-2D run.

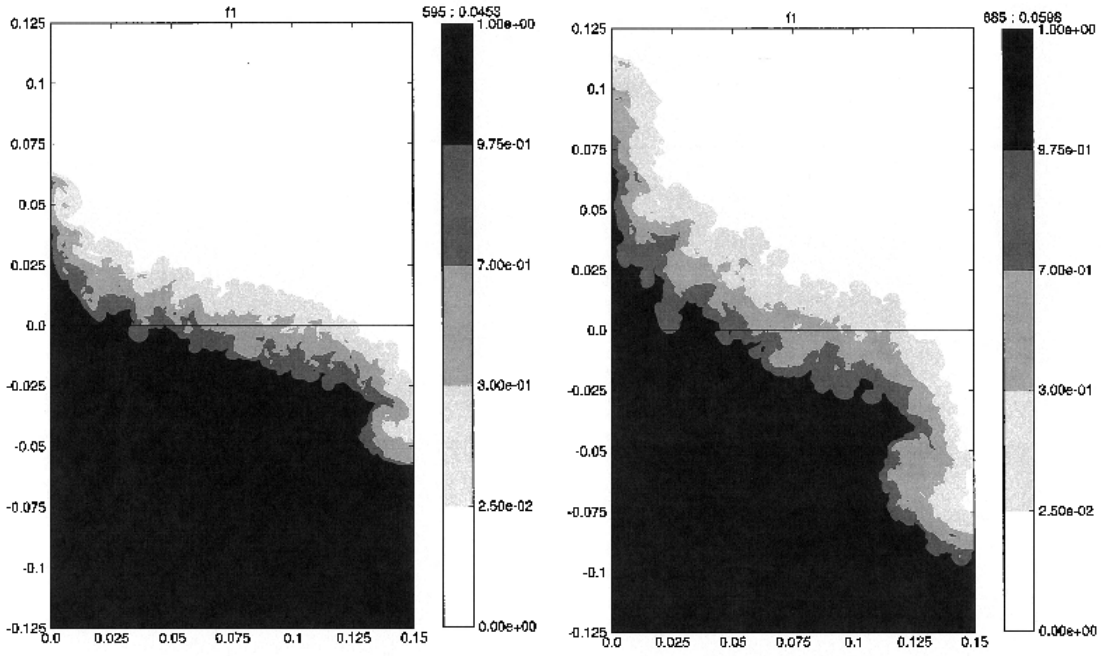

Figure 21: CFDNS f_1 contours at a) τ= 1.256 and b) τ= 1.741.

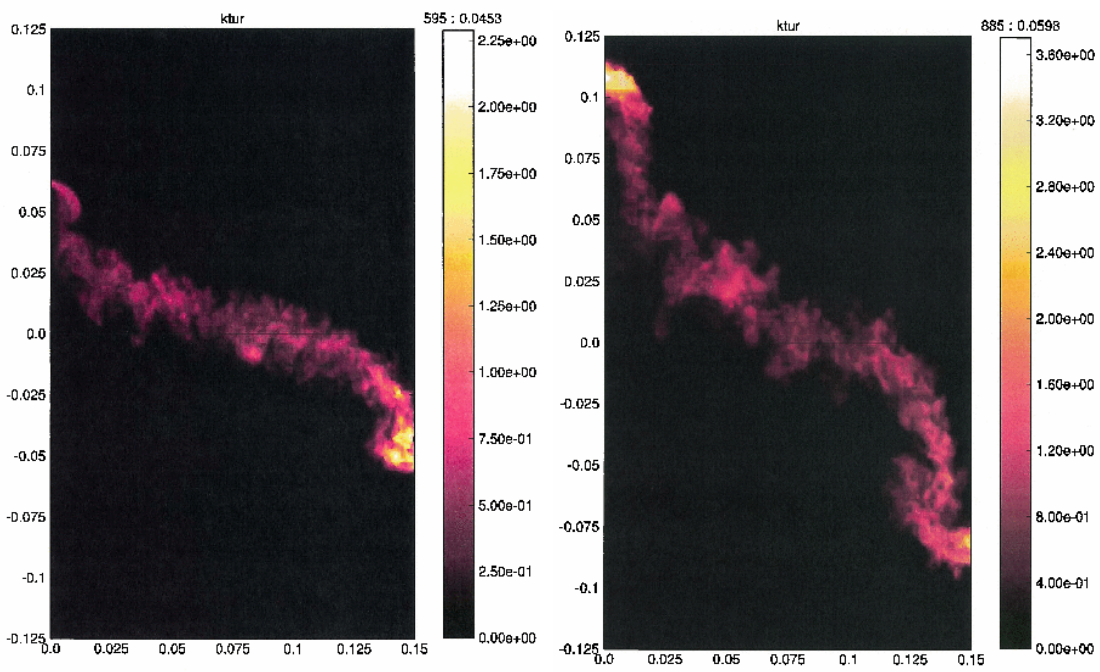

Figure 22: CFDNS turbulent kinetic energy (m^2/s^2) at a) τ= 1.256 and b) τ= 1.741.

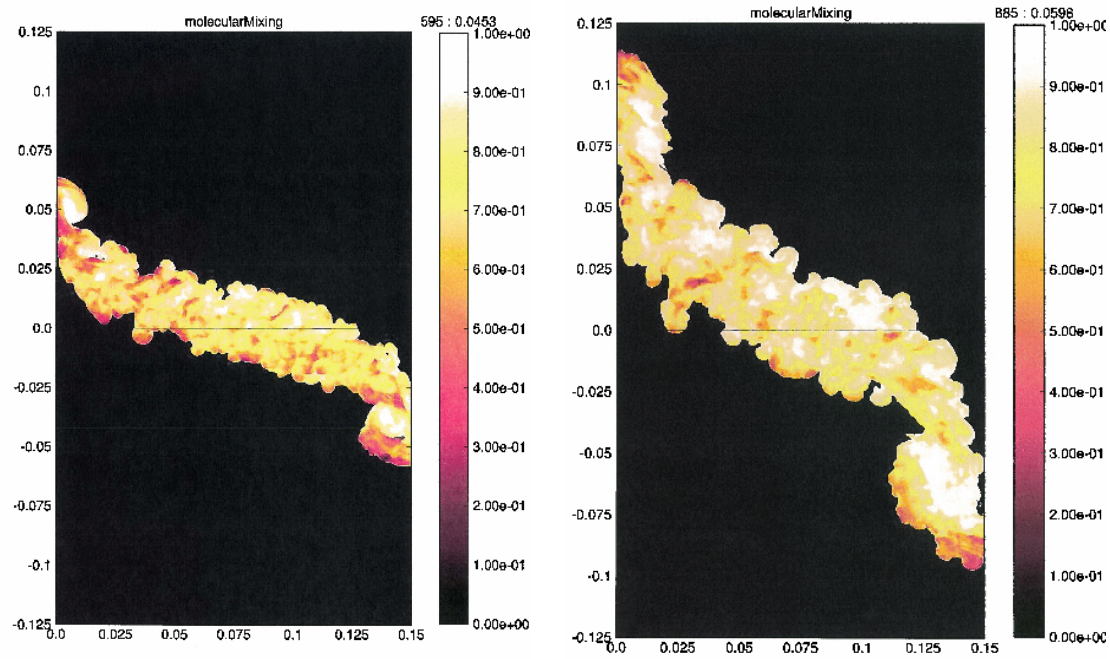

Figure 23: CFDNS molecular mix parameter at a) τ=1.256 and b) τ= 1.741.

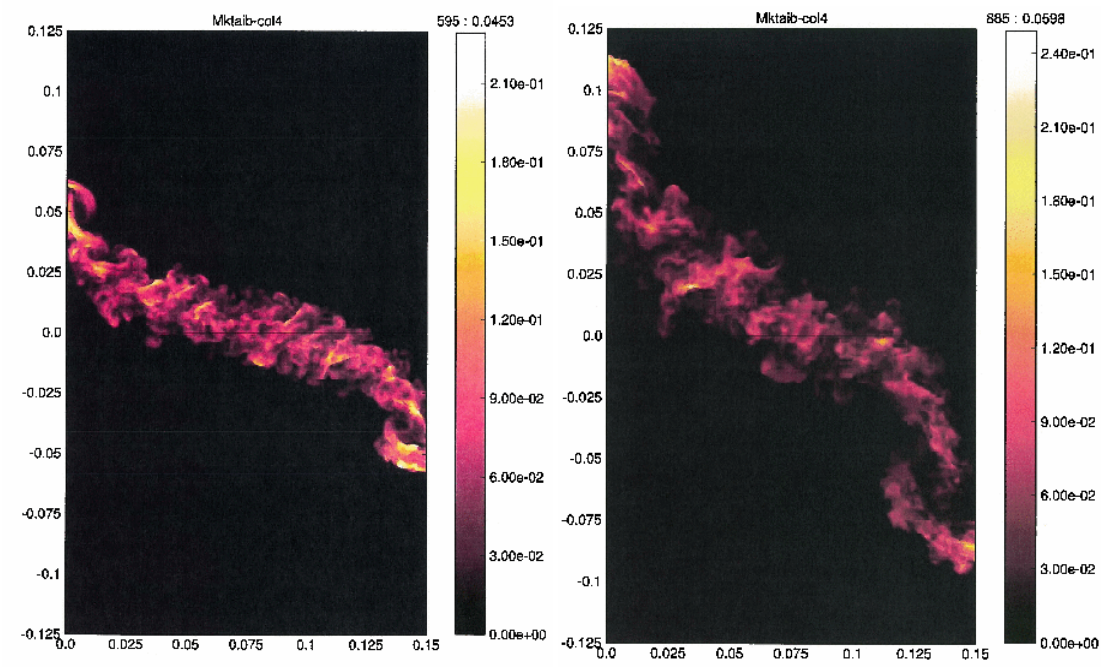

Figure 24: CFDNS density specific volume correlation b at a) τ=1.256 and b) τ= 1.741.

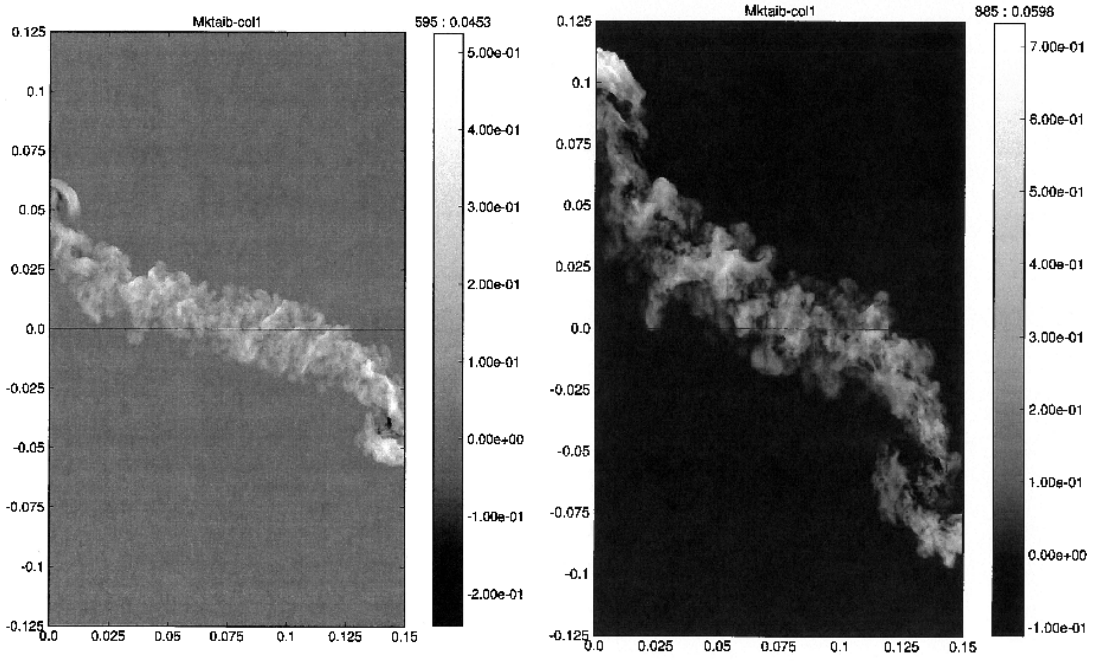

Figure 25: CFDNS vertical mass flux (m/s) at a) τ=1.256 and b) τ= 1.741.

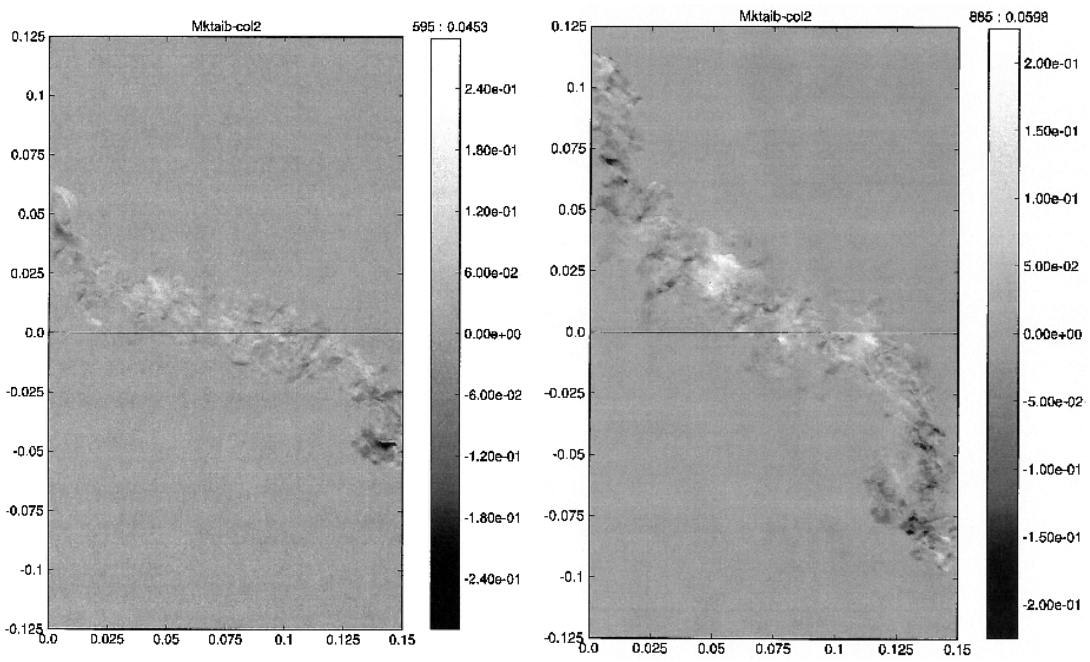

Figure 26: CFDNS horizontal mass flux (m/s) at a) τ=1.256 and b) τ= 1.741.

Figure 27. Comparison of molecular mixing